

# The Nature of Strange Modes in Classical Variable Stars

J. R. Buchler @1\*, P. A. Yecko @1\*\*, Z. Kolláth @1 @2\*\*\*

@1 Physics Dept., University of Florida, Gainesville FL32611, USA @2 Konkoly Observatory, Budapest, Hungary

January 1997

**Abstract.** Strange modes have been found in the radial spectrum of many luminous stars, such as PAGB stars. The strange modes are characterized by having small amplitudes in the interior of the envelope, and egregious periods and growth-rates. It has been common belief that the strange modes are a result of strong nonadiabaticity. Recently, and perhaps surprisingly, such modes have also been found in classical Cepheid models, even though these are weakly nonadiabatic stars. Here we show that in fact there is nothing strange about these modes and that they must exist even in the adiabatic limit. They are essentially acoustic surface modes.

By means of a simple change of variables and *without approximation*, the adiabatic linear pulsation equation for the radial displacement is reduced to a Schrödinger like equation in which the radial coordinate is the local sound traversal time. In this formulation, the narrow hydrogen partial ionization region is seen to act as a potential barrier, separating the star into two regions. Modes can be trapped either in the inner or in the surface region. Coupling through the barrier gives rise to resonances between the inner and surface regions. The strange modes are those in which the ratio of inner to surface amplitude is at a minimum. The potential problem formulation shows that strange modes exist in the adiabatic limit. As a function of the stellar parameters the relative location of the barrier changes, and this gives rise to the phenomenon of *avoided level crossings* along a sequence of models.

The appearance of strange modes and the associated level crossings can be exhibited with an *analytically* solvable toy model when the potential barrier is approximated by a delta function. In the full nonadiabatic models the same trapping mechanism remains responsible for the appearance of strange modes. The unusual growth-rates are seen to also be a consequence of the relative minimum of the inner amplitude for these modes. Again the behavior of the nonadiabatic modes can be well mimicked by a simple analytical toy model.

The strange modes can be linearly unstable to the left of the fundamental and first overtone blue edges. Hydrodynamical calculations show that the strange limit cycle pulsations (a) are extremely superficial as the linear eigenvectors already indicate, in fact they have negligible amplitudes interior to the partial hydrogen ionization front, and (b) the pulsations have surface radial velocities in the 0.1 – 1.0 km/s range, but extremely small photospheric velocities, and luminosity variations in the milli-magnitude range. These modes are therefore expected to be difficult to observe.

**Key words:** stars: variables: Cepheids – stars: oscillations

## 1. Introduction

This work sets out to demystify the so-called strange vibrational modes that are regularly encountered in stars with high luminosity to mass ratio, such as PAGB stars (Cox et al. 1980, Saio et al. 1984, Aikawa 1985, Gautschy & Glatzel 1990, Zalewski 1992, 1994, Cox & Guzik 1996, Papaloizou et al. 1997), but more recently also in Cepheids (Buchler 1997) where they were not expected because of the weakly nonadiabatic nature of the pulsations in these stars. We begin in §2 by rephrasing the description of adiabatic pulsations in the general form of a quantum mechanical potential well problem. The natural follow-up is to focus on the resulting potential. This we do for a Cepheid and find that the sharpness of the hydrogen ionization front produces an immensely high barrier in the potential, effectively separating the star into two distinct regions. The barrier is ultimately caused by the rapid variation of the local sound speed, most by the adiabatic index. In §3, for didactic purposes, we present a toy problem that approximates the Cepheid, yet contains all the essential features of strange modes, and that can be solved analytically. We thereby verify that the first appearance of a strange mode occurs in concert with a node crossing the potential barrier into the narrow outer envelope of the star between the surface and the hydrogen partial ionization region (HPIR).

\* e-mail address: buchler@phys.ufl.edu

\*\* e-mail address: yecko@phys.ufl.edu

\*\*\* e-mail address: kollath@buda.konkoly.hu

In §4 we look in detail at a specific Cepheid model, using the transformations inspired by the potential well formulation set out in §2. An entire sequence of Cepheid models is then examined in §5, and the signature of strange modes is revealed unequivocally. It will become apparent that the gradual change in the model parameter, which affects the extent of the region between the HPIR and the stellar surface, modifies the resonance conditions between the inner and outer regions and is responsible for the observed systematic changes along the sequence. In §6 we extend the adiabatic toy model of §3 to the nonadiabatic case by allowing a complex potential barrier. Although we show this model to be highly approximate, it does reproduce the behavior of the periods and of the growth-rates in Cepheid sequences quite accurately.

The pulsating stellar envelope, both physically and mathematically, bears a strong resemblance to a (quarter wave length) flared wind instrument such as a horn or trumpet. In §7 we explore this analogy and design an *equivalent musical wind instrument* with the characteristics of the Cepheid spectrum.

The strange modes can be unstable outside the usual Cepheid instability strip and can thus give rise to nonlinear pulsations of their own. In order to shed some light on the appearance of such pulsations and answer the question of their observability we therefore compute the nonlinear hydrodynamical behavior of several such “Cepheid” models in §8.

## 2. The Cepheid Potential

In the standard equilibrium radiative diffusion approximation adiabatic radial pulsations are described by the familiar equation for the radial displacement eigenfunctions  $\delta r$ :

$$\frac{\partial^2}{\partial t^2}(r^2\delta r) = \frac{r^2}{\rho} \frac{\partial}{\partial r} \left[ \frac{\Gamma_1 P}{r^2} \frac{\partial}{\partial r}(r^2\delta r) \right] + \frac{4GM}{r^3} r^2 \delta r. \quad (1)$$

where the symbols have their usual meanings (e.g. Cox 1980).

We can recast the description of the adiabatic pulsation problem in terms of a new function  $\Phi$  by invoking the transformation

$$\Phi = (\Gamma_1 P)^{\frac{1}{2}} r \delta r = (\rho)^{\frac{1}{2}} c_s r \delta r, \quad (2)$$

where the second equality simply involves the adiabatic sound speed:  $c_s^2 = \Gamma_1 P / \rho$ . Thus

$$c_s^2 \frac{d^2 \Phi}{dr^2} + W(r)\Phi = \omega^2 \Phi, \quad (3)$$

where the assumed  $\exp(-i\omega t)$  time dependence has allowed us to replace the temporal derivative by the eigenvalue  $\omega^2$ , and the function  $W(r)$  is given by

$$W(r) = \frac{1}{(\rho^{\frac{1}{2}} c_s / r)} \frac{d^2}{dr^2} (\rho c_s^2 / r^2)^{\frac{1}{2}} - \frac{4GM}{r^3}. \quad (4)$$

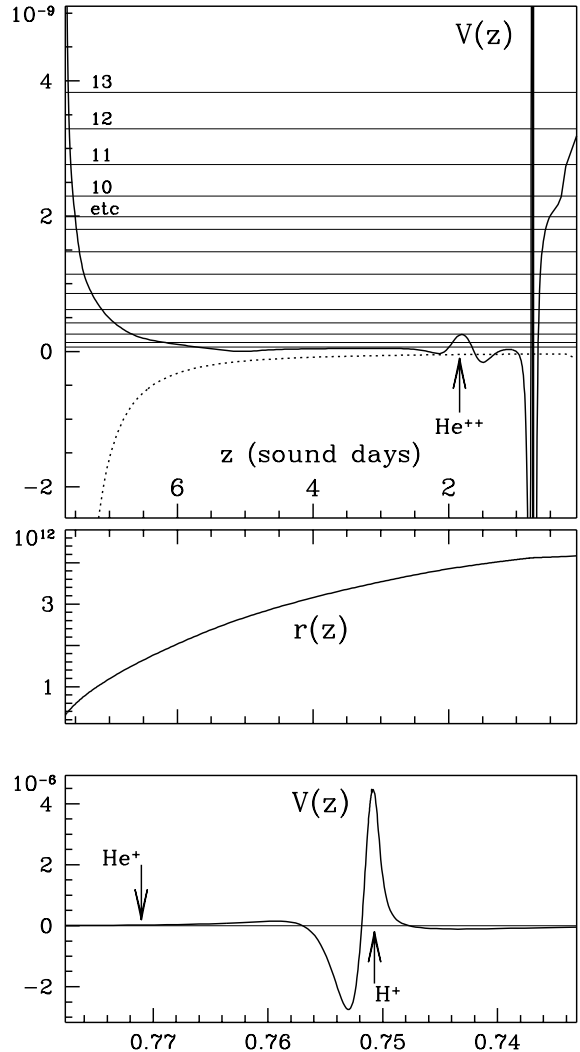


**Fig. 1.** Effective potential for the adiabatic pulsations; top: full potential (solid line) and gravitational contribution (dotted line); the horizontal lines denote the lowest eigenvalues  $\omega_n^2$ ; middle: scale transformation  $r(z)$ ; bottom: blow-up of the region near the hydrogen partial ionization region; Stellar surface is on the right at  $z = 1$ .

The first term of  $W(r)$  embodies the effects of the spatially varying inertia (density) and sound speed on  $\Phi$ , and the form it takes is a result of applying Eq. (2) to Eq. (1). Anywhere the equilibrium varies rapidly,  $W(r)$  is dominated by this first term. The second term of  $W(r)$  results from the variation of gravitational forces within the hydrostatic equilibrium and will only be important at small radius and for modes with small wave number (these have local wavelengths comparable to the scale for which the gravitation varies). Both terms play a role in determining the global frequency spectrum of radial modes.

We note in passing that when a plane-wave function  $\Phi(r) = \exp(ikr)$  is inserted, Eq. (3) then represents the local dispersion relation and can be used to construct a *propagation diagram* (Unno et al. 1989).

We can now go one step further and convert Eq. (3) into a Schrödinger like equation by eliminating the sound speed that modifies the spatial derivative in Eq. (3); we do this by transforming from  $r$  to a new coordinate  $z$ , chosen to increase inward:

$$dz = -dr/c_s. \quad (5)$$

The quantity  $z$  then represents the *acoustic depth* (or sound traversal time) and is conveniently measured in *sound days* here ( $r(z)$  appears in Fig. 1, center panel). The newly phrased problem involves a concomitant transformation of the eigenfunctions according to:

$$\Psi = (\rho c_s)^{\frac{1}{2}} r \delta r = c_s^{-\frac{1}{2}} \Phi \quad (6)$$

which converts Eq. (1) into

$$-\frac{d^2}{dz^2} \Psi + V(z) \Psi = \omega^2 \Psi, \quad (7)$$

where the potential is given by

$$V(z) = \frac{1}{(\rho c_s/r^2)^{\frac{1}{2}}} \frac{d^2}{dz^2} (\rho c_s/r^2)^{\frac{1}{2}} - \frac{4GM(\rho c_s)^{\frac{1}{2}}}{r^4}. \quad (8)$$

Note that the potential  $V$  in Eq. 7 differs from  $W$ .

Eq. (7) is clearly the simplest and most compact form that the problem of adiabatic stellar pulsations can be expressed in. The spatial gradients of the equilibrium quantities  $\rho$  and  $c_s$ , as well as sphericity effects have been incorporated into the modified eigenfunctions  $\Psi$  and into the transformed spatial coordinate  $z$ . The effective sound speed is therefore unity and we can set  $\omega = k$ , the wavevector. The boundary conditions associated with the original problem Eq. (1) are readily transcribed to the new formulation of Eq. (7).

Eq. (7) has been derived for the radial displacement eigenvector, or equivalently the velocity. In the literature one also finds equations similar to Eq. (3) or (7), but for the pressure eigenfunction  $\delta p$  (e.g. Deubner & Gough 1984). We stress that the derivation for such a Schrödinger equation for  $\delta p$  is only possible if approximations are made. The exact equation for  $\delta p$  would involve third order spatial derivatives, unless the variations of the gravitational potential are neglected in the linearization (Cowling approximation).

We now examine the potential of a specific Cepheid model, choosing the parameters  $L = 3000L_\odot$ ,  $M = 5M_\odot$ ,  $T_{\text{eff}} = 5520\text{ K}$ ,  $Z = 0.02$ ,  $X = 0.70$ . We use the latest OPAL opacities (Iglesias & Rogers 1996) with Alexander-Ferguson (1994) molecular opacities. Convection is ignored.

The top panel of Fig. 1 displays  $V(z)$  (heavy solid line) and its gravitational component (dotted line) for this Cepheid model. The gravitation contributes a small, but significant depth in the interior. In this plot the coordinate  $z$  ranges over the entire pulsating envelope. The scale of  $z$  is of the same order as the period of the gravest pulsational modes (cf. virial theorem). In order to reveal the overall structure of the potential well the vertical scale is highly magnified. The horizontal lines indicate the relative placement of the adiabatic pulsation energies. The barrier at  $z = 0.75$  is so high as to be off-scale and so narrow as to be featureless with respect to the scales that are appropriate for the pulsations. Therefore in the bottom panel of Fig. 1 we exhibit the shape of the potential  $V(z)$ , restricting our perspective here to a very narrow region in the vicinity of the HPIR.

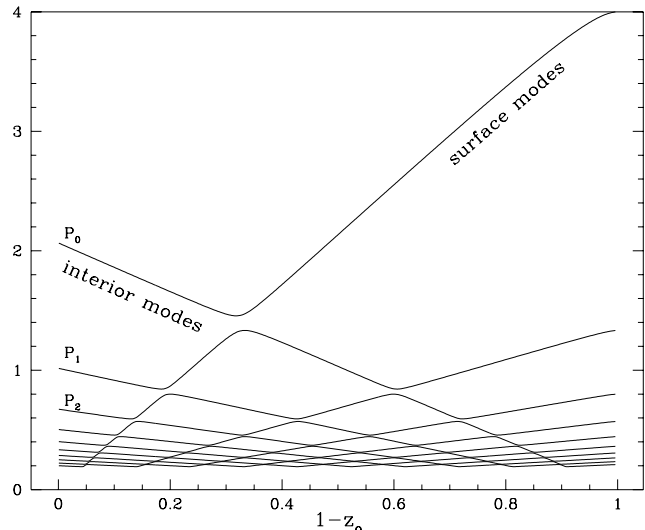


**Fig. 2a.** Periods of the barrier problem, with  $V_0=10$ ;  $z_0$  is the distance of the barrier from the inner (nodal) boundary;  $1-z_0$  is thus the width of the outer region.

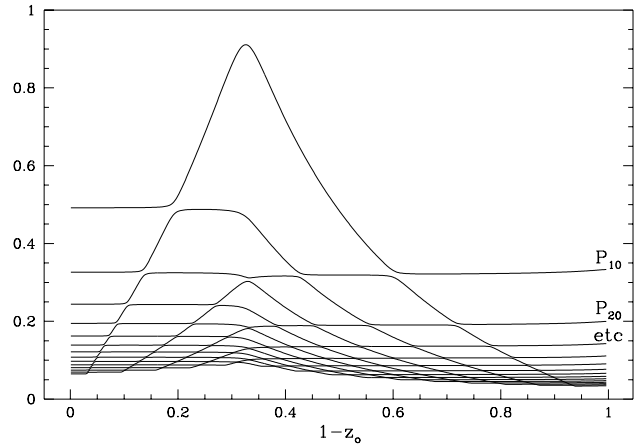


**Fig. 2b.** Period ratios of the barrier problem, with  $V_0=10$ ;  $1-z_0$  is the width of the outer region.

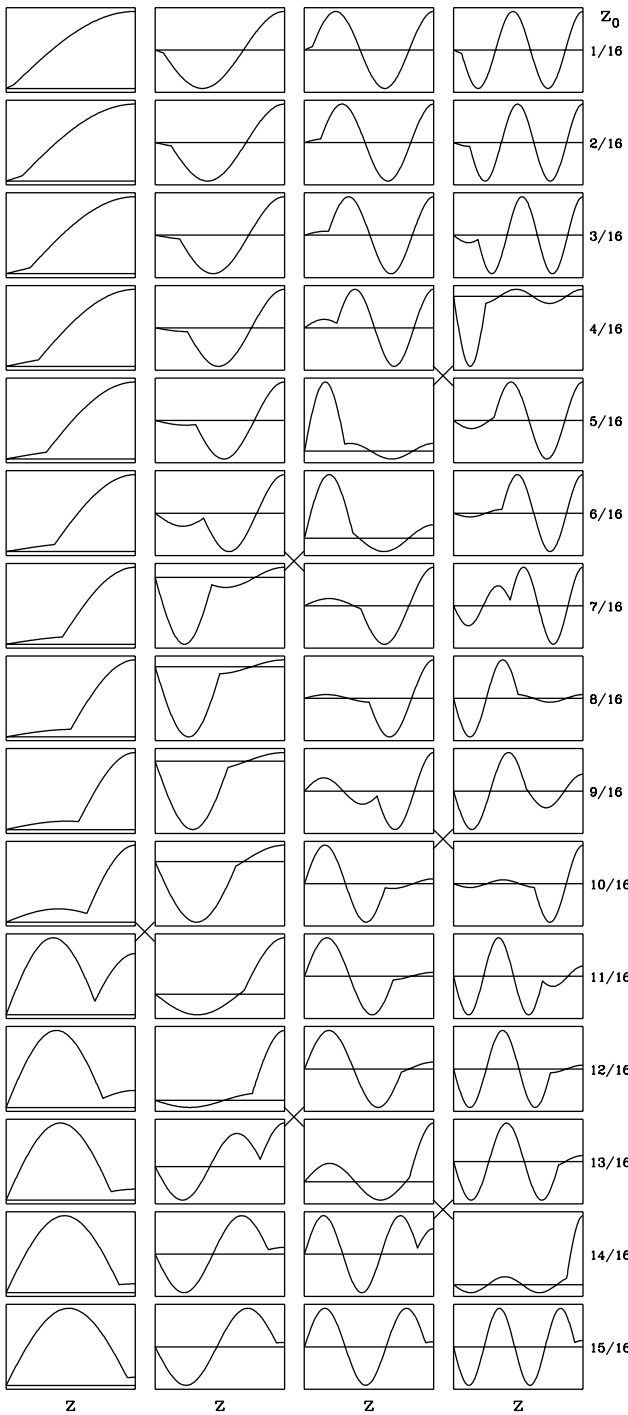


**Fig. 3.** Lowest four eigenfunctions as a function of barrier location  $z_0$ , with  $V_o=10$ ;  $1-z_0$  is the width of the outer region.

The middle panel of Fig. 1 plots the relation between the radial coordinate  $r$  and the acoustic depth  $z$ . In the new  $z$  coordinate the inner regions with their high sound speed now appear highly compressed. We have adopted zero acoustic depth ( $z = 0$ ) at the stellar surface.

Of the three quantities that appear in the second derivative of Eq. 8, it is the sound speed whose variations are most significant. Recall that  $c_s \propto \Gamma^{\frac{1}{2}}$  and  $\Gamma$  experiences rapid dips (e.g. Cox & Giuli 1968) in ionization zones that then produce the large potential fluctuations. The centers of the three ionization stages,  $H-H^+$ ,  $He-He^+$ ,  $He^+-He^{++}$  are indicated by arrows in Fig. 1. Of these it is the hydrogen that is by far the narrowest, leading to a potential barrier.

### 3. An Idealized Potential Barrier Toy Problem

For a potential like that shown in Fig. 1 the eigensolutions have many properties that can be demonstrated in a more transparent way by looking at a toy problem. This toy problem can be solved analytically, yet it displays the essential features of the modal spectrum of the star. We replace the actual potential with an infinitesimally narrow barrier (a delta function of strength  $V_o$ ) which is located at  $z_o$  ( $0 < z_o < 1$ ) and the potential simply zero elsewhere. Thus the Schrödinger equation reduces to

$$-y'' + V_o k \delta(z - z_o) y = \omega^2 y. \quad (9)$$

where  $k \delta(z - z_o)$  models the potential shape and  $V_o$  is a dimensionless scale factor. We choose the boundary conditions appropriate for the adiabatic pulsations of a Cepheid, those for a quarter wave-length tube that is closed at the inner boundary and open at the outer (pure reflection), *viz.* :

$$y(0) = y'(1) = 0. \quad (10)$$

The eigenvectors are given by

$$\begin{aligned} y(z) &= a \sin kz & z \leq z_o \\ &= \cos k(1-z) & z_o \leq z \end{aligned} \quad (11)$$

with normalization  $y(1) = 1$  (more generally  $a(k) = y'(0)/ky(1)$ ). With the appropriate matching conditions

$$y(z_o^+) = y(z_o^-) \quad (12a)$$

$$y'(z_o^+) = y'(z_o^-) + k V_o y(z_o), \quad (12b)$$

one obtains the characteristic equation for  $k$

$$\cos k + V_o \sin kz_o \cos k(1-z_o) = 0. \quad (13)$$

The inner amplitude  $a$  is given by

$$a(k) = \cos k(1-z_o)/\sin kz_o. \quad (14)$$

We note several interesting features. First, Eq. 13 shows that for large  $V_o$  (a very high barrier) one obtains  $\cos k(1-z_o) \sin kz_o \approx 0$ . Thus for  $z_o \rightarrow 0$  (vanishing inner region) the spectrum is given by  $\cos k = 0$ , with periods  $P_n = 4/(2n+1)$ , i.e. the one of an open tube, whereas for  $z_o \rightarrow 1$  (vanishing outer region) we have essentially a closed tube and its spectrum  $\sin k = 0$  with  $P_n \approx 2/(n+1)$ .

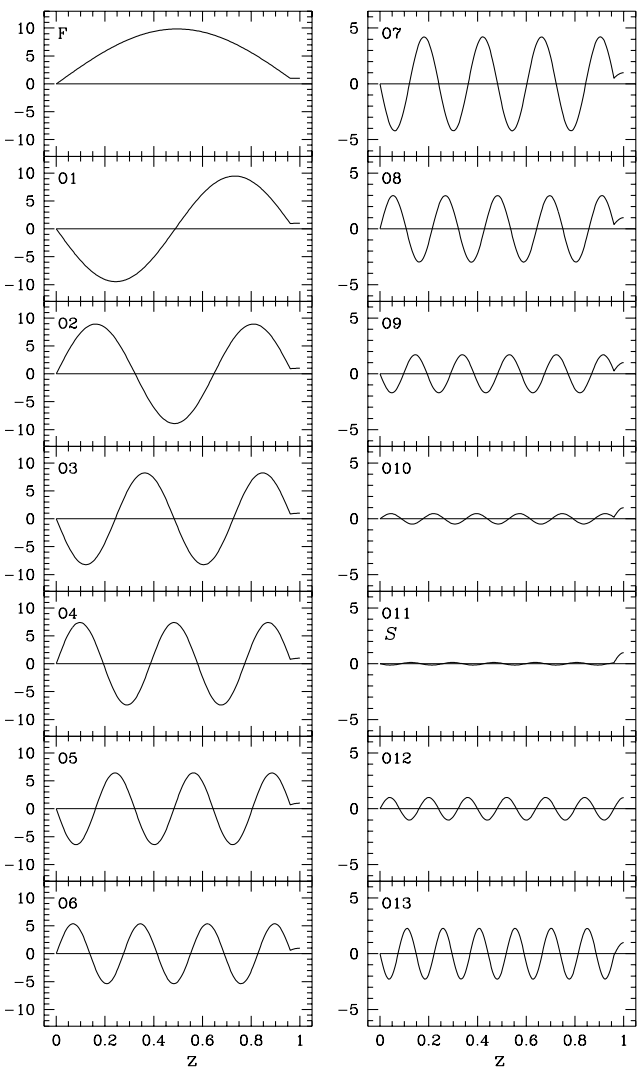


**Fig. 4.** Eigenvectors  $y_n$  of the potential barrier toy problem with  $z_o = 0.96$  and with  $V_o=10$ ; the strange mode is labelled  $S$ .

This asymptotic behavior in  $z_o$  is nicely seen in Fig. 2a that shows the period spectrum as a function of  $1-z_o$  for a value  $V_o=10$ . (The reason for plotting versus  $1-z_o$  instead of  $z_o$  is that we eventually compare to fig. 10 in which the outer acoustic distance increases with  $P_0$ .) Following common practice we assume that the modes are ordered by decreasing periods  $P_n$ .

A null inner amplitude can occur for specific combinations of  $V_o$  and  $z_o$ , i.e. nongenerically, as Eq. (14) shows. We call these modes perfect surface modes. It will be seen later in the application to stars that the surface modes are in fact the strange modes. For arbitrary values of  $V_o$  and  $z_o$  we refer more loosely to the mode whose amplitude is at a minimum as the strange mode.

The outer boundary condition precludes a zero outer amplitude, i.e. infinite values of  $a$ , but  $a$  can get very large. We refer to the corresponding modes as *inner modes*; later

we shall see that in stars the inner modes are the *regular modes*.

Finally, in between the inner and the outer modes lie modes that have a uniform amplitude throughout ( $a=1$ ). Such perfectly matched modes can occur accidentally when a node happens exactly at  $z_o$  (cf. Eq. 12b). For most values of  $V_o$  and  $z_o$  one can generally identify modes that are close to being matched.

It is amusing to notice in Figs. 2a and 2b how, through the intermediary of trapped modes, the spectrum gradually changes from that of a closed to an open tube as  $1-z_o$  varies between 0 and 1. The reason for this, as we have seen, is that a very strong barrier (large  $V_0$ ) acts almost like an additional interior boundary condition. Below the barrier, the modes resemble those of a closed pipe of length  $z_o$ , while above the barrier the modes resemble those of an open pipe of length  $1-z_o$ . Except for the rare situation of matched modes, either the inner or the outer amplitude dominates, i.e. the modes are either inner (regular) or outer (strange) modes.

The appearance and behavior of the modes is further, and more globally illustrated in Fig. 3 which shows the lowest three eigenvectors as a function of  $z$ . We recall that the closed end is on the left ( $z = 0$ ) and the open end on the right ( $z = 1$ ). In the right margin we show the location of the barrier  $z_o$ . This figure should be looked at in conjunction with Fig. 2a which shows the periods  $P_n$  as a function of  $z_o$ .

Consider first the fundamental mode displayed in the leftmost column of Fig. 3. As expected, for small  $z_o$  the outer well dominates and the eigenfunction is essentially that of an open, quarter-wavelength tube. As the barrier moves to the right, the effective length of the tube shrinks, causing a decrease in the period as seen in Fig. 2a. On the other hand, starting from the bottom, we see that the eigenfunction is now essentially that of a closed half wavelength tube with half the period of the  $z_o = 0$  case. For  $z_o=2/3$  one can fit exactly  $3/4$  of a wavelength into the well, which corresponds to a perfect match condition. At the shown values of  $z_o=10/16$  and  $11/16$  the  $y_0$  eigenvectors are indeed very close to those of the first overtone of an open tube, but being the fundamental mode they avoid acquiring a node. This is also the place where a near degeneracy occurs as Fig. 2a indicates. However, because the Sturm-Liouville nature of the problem precludes degeneracy, there must be an avoided level crossing. (Strictly speaking, the problem is not Sturm-Liouville because of the  $\delta$  function potential, but seems to preserve the features thereof in this singular limit). If we look at the second column which represents the first overtone in the well we notice that the system avoids degeneracy through a switchover between the fundamental and the first overtone, indicated in Fig. 3 by the X linking columns 1 and 2. There is of course nothing special about the fundamental and first overtone, and we see similar avoided crossings in

Fig. 4 and corresponding switchovers in the eigenvectors in Fig. 3 that are also indicated by crosses.

The lines with a positive slope in Fig. 2a correspond to modes with predominant amplitudes in the outer well, i.e. with open tube characteristics, whereas the those with negative slope have predominant amplitudes in the inner well, i.e. are essentially closed tube modes. It is thus the overlap of the open and closed tube spectra that makes up the pattern of Fig. 2a.

The shapes of the fundamental eigenvectors in Fig. 3 show that changing  $z_o$  is essentially equivalent to changing the length of the tube, and explain why the periods increase/decrease linearly with  $z_o$ .

The periods  $P_n$  change with  $z_o$ , but the ratios  $P_{n0}$  are almost everywhere independent of  $z_o$  and thus straight lines. The reason for this near constancy is again that changing  $z_o$  changes the equivalent length of the tube. We show the period ratios in Fig. 2b so that later they can be compared to those of the Cepheid model sequence.

Why do the modes alternate between inner and surface modes? Consider again Fig. 3, column 1 starting at the bottom and going up. Near the open end the eigenvector is forced to bend down, at a constant rate because the curvature of  $y$  is given by  $-k^2 y$ . Therefore the slope of the eigenvector in the outer region gets increasingly steep as the barrier location moves inward. Since there must be a finite, fixed change in slope at  $z_o$  (Eq. 12b) the slope of the eigenvector of the inner region is increasingly flattened, thus suppressing the inner amplitude (which has to go to zero at  $z_o=0$ ). The overtone modes follow the same scenario.

We now examine more closely the case with parameter values  $z_o = 0.96$  and  $V_o = 10$  that approximately mimics the Cepheid situation. Eq. (13) is easily solved and the the lowest 14 modes eigenvectors  $y_n$  are displayed in Fig. 4 vs. acoustic depth  $z$ . Referring back we see that this puts us on the extreme left of Fig. 2. We note in particular that the strange (surface) mode is expected to appear only for large mode number. Indeed, Fig. 4 shows that here it is mode O11 that is strange (and mode O12 that is nearly matched). Note that for mode O12 a node occurs very close to  $z_o$  which then causes no jump in the slope (Eq. 13). Modes higher than O12 therefore have at least one node in  $z_o < z \leq 1$ .

One can again look at the behavior of the modes in Fig. 4 in terms of matching of the eigenvectors through the potential barrier. Here now the curvature increases with modal index (wave number  $k$ ). For the lowest modes the curvatures and bending down of the eigenvectors are small and the modes are inner (regular) modes. As mode O9 is approached the matching has already started to seriously suppress the inner amplitude which reaches a minimum for O11 which is the surface (strange) mode. Note that both O10 and O12 have approximately the same inner and outer amplitudes and are hybrid modes. For mode O12 furthermore the node occurs very close to the

barrier location  $z_o$  and O12 is thus an almost perfectly matched mode. The subsequent modes become again regular modes, and through the same mechanism a new surface mode appears. This whole scenario repeats itself with a relative recurrence period of  $\approx 1/(1 - z_o)$  in the modal index (cf. Eq. 14).

As a byproduct of the previous paragraph we note that the minimal amplitude and the near match occur very close to each other, and that both phenomena are the consequence of a near resonance between the inner and outer potential wells.

The connection with the usual stellar modes will become more apparent when we consider the behavior of the  $\delta r_n$  rather than the  $\Psi_n$  in the next section.

Thus in the Cepheid case the radial vibrational modes that are confined to the surface regions have strange properties. Under cross-over conditions both modes are an admixture of normal and strange modes. This is of course not all that different from what happens for nonradial Main Sequence stars where different mode types,  $g$  and  $p$  modes, are involved in the level crossings (e.g. Unno et al. 1989).

#### 4. Details of a Cepheid Model

Before discussing the strange modes in sequences of nonadiabatic Cepheid models where they were first noticed (Buchler 1997) we first return to the Cepheid model of §2 in order to show how the toy problem of §3 serves as a perfect paradigm for explaining the nature of the strange mode.

We have to be a little bit careful with the outer boundary condition because of the almost isothermal nature of the outer region. In order to avoid problems we define the surface as the point where the density is small, but nonzero, or more conveniently where the pressure is equal to some small value  $p_*$ , say two times the radiation pressure ( $aT^4/3$ ). We impose this  $p_*$  as a constant outer pressure in the subsequent dynamics. (The exact value of this pressure is not critical).

##### 4.1. The Adiabatic Cepheid Model

A great deal can be learned by examining the linear pulsations in the adiabatic limit, i.e. we ignore the entropy variations during the pulsation.

The adiabatic displacement eigenfunctions  $\Psi_n$  for the first fourteen pulsational modes are shown in Fig. 5, starting with the fundamental mode (F). With increasing  $k$  a node moves outward toward  $z_o$  and, as overtone mode O11 is approached, the node is about to reach  $z_o$ . The similarity with the analytical toy-model of the previous section is striking. As in the toy problem, the inner amplitude decreases to a minimum, – the property that has been used to identify a strange mode. There is no doubt that in an actual Cepheid model the occurrence of the strange mode

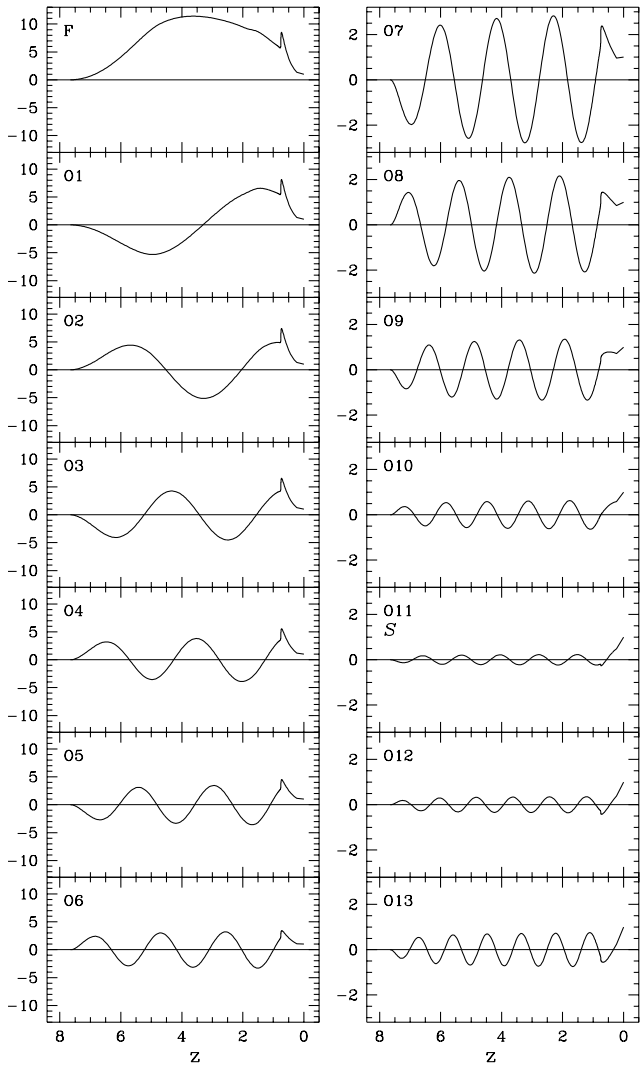


**Fig. 5.** Adiabatic eigenvectors of the scaled displacement  $\Psi_n$  vs. acoustic depth for the Cepheid Model; the strange mode is labelled by  $\mathcal{S}$ .

is also the result of the confinement of the mode to the outer cavity of the potential well.

There are some small differences with the toy problem, for example in the detailed behavior both near  $z = 1$  and through the potential barrier. This is not astonishing considering that in the toy model we ignored the potential dip near  $z = z_0$  as well as the broad, but relatively low potential barrier near  $z = 1$  (The effect of the latter is seen in the exponential behavior of the low modes near the surface).

It is interesting of course to compare the scaled eigenfunctions  $\Psi_n$  to the radial eigenfunctions  $\delta r_n$  which are shown in Fig. 6. The scale factor  $(r\sqrt{\rho c_s})^{-1}$  in Eq. 6 greatly magnifies the surface region and the strange mode now appears even more as a surface trapped mode.

While the radial displacement eigenfunction  $\delta r_n$  has perhaps a more physical meaning, the  $\Psi_n$  representation

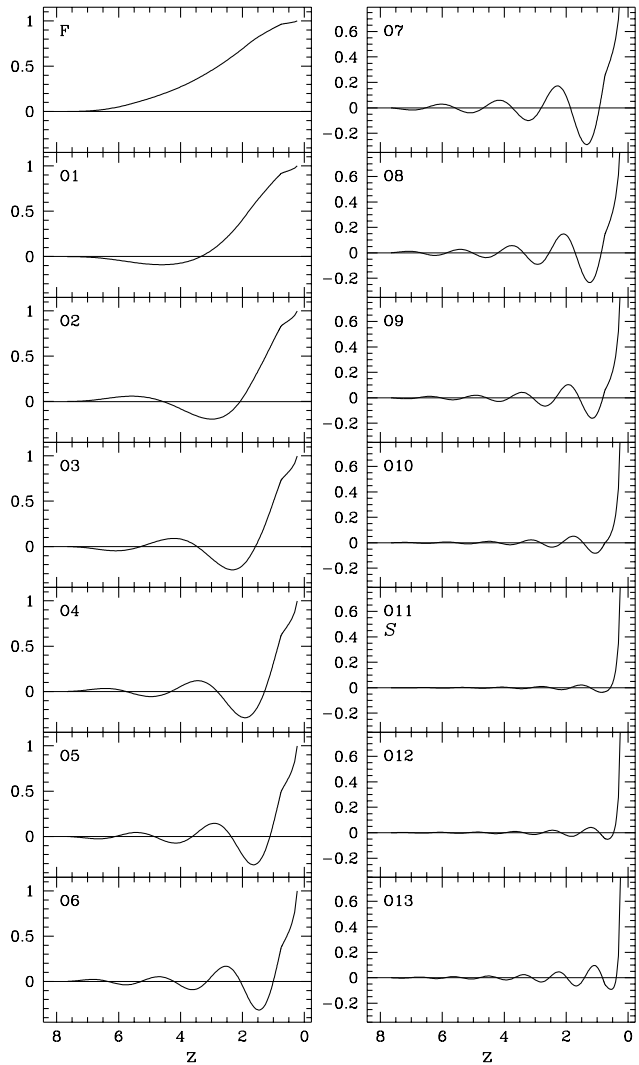


**Fig. 6.** Adiabatic eigenvectors  $\delta r_n/r$  vs. acoustic depth for the Cepheid Model; note the different scales on the left and on the right column. The strange mode is labelled by  $\mathcal{S}$ .

provides an optimal scaling of the problem, and is perhaps more basic from a mathematical point of view. It shows in particular that even for a strange mode the inner regions play an important role even though in  $\delta r_n$  all modes appear to be surface modes.

We conclude that a *strange adiabatic mode* has its origin in the potential barrier that is created by the ionization front of hydrogen in the outer envelope. It first appears when, with increasing mode number, an actual node is forced to occur near the surface (outside the HPIR). This then pushes down the inner amplitude of the mode to a very low value. The new, interesting point is that the strange mode already appears in the adiabatic limit.

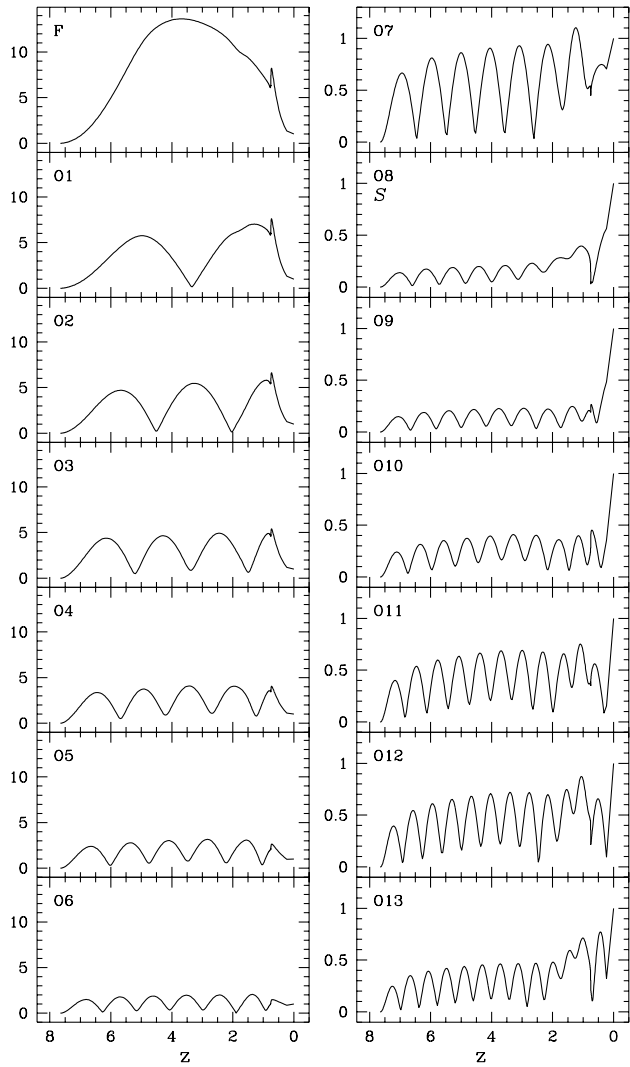


**Fig. 7.** Nonadiabatic eigenvectors  $|\Psi_n|$  vs. acoustic depth for the Cepheid Model; the strange mode is labelled by  $\mathcal{S}$ ; note the different scales on the right and left.

#### 4.2. The Nonadiabatic Model

We now turn to the correct, *nonadiabatic* linearization of the Cepheid model. In Fig. 7 we display the moduli of the *nonadiabatic* displacement eigenvectors  $\Psi_n$ , related to the radial eigenvectors through the scaling of Eq. (6), and normalized to 1 at the surface. Juxtaposed we show in Fig. 8 the corresponding radial displacement eigenvectors  $|\delta r_n|/r$ . The nonadiabaticity is weak for Cepheids ( $\kappa_n \ll \omega_n$  for the low modes) and therefore the properties of the nonadiabatic eigenvectors to a large extent mimic those of the adiabatic problem. (We recall that in our notation the eigenvalues for an assumed  $\exp(\sigma_n t)$  dependence are denoted by  $\sigma_n = i\omega_n + \kappa_n$ .)

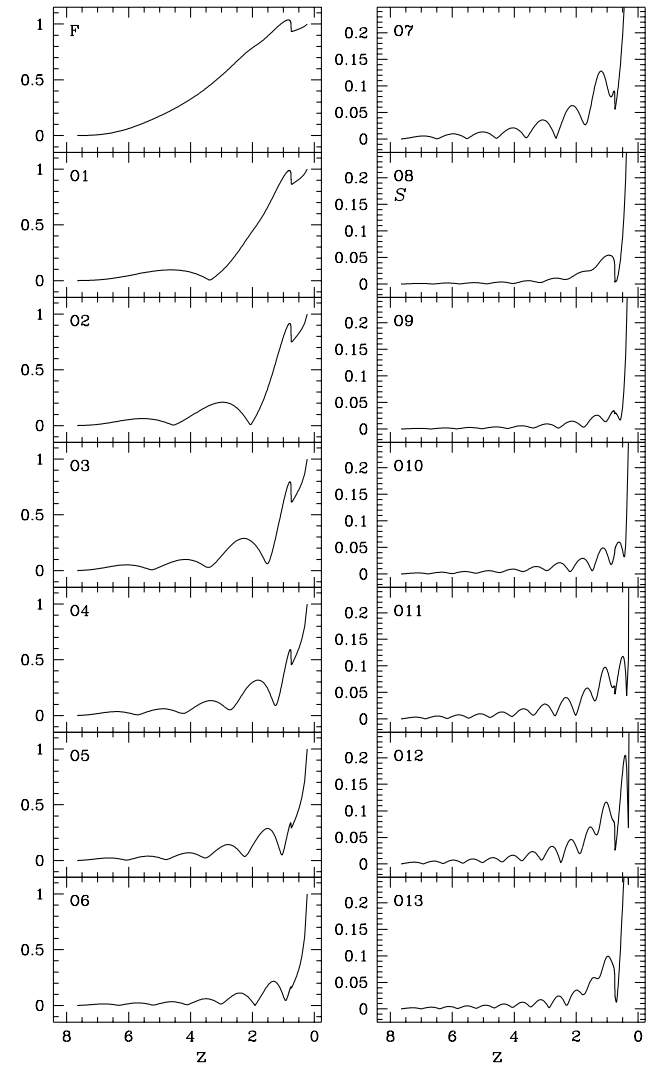


**Fig. 8.** Nonadiabatic eigenvectors of the scaled displacement  $|\delta r_n|/r$  vs. acoustic depth for the Cepheid Model; the strange mode labelled by  $\mathcal{S}$ ; note the different scales on the right and left.

#### 4.3. Transition From Adiabatic to Nonadiabatic Model.

The nonadiabatic spectrum is noticeably different from the adiabatic one as Table 1 shows, in particular it is mode 08 which is now the strange mode (denoted by the symbol  $\mathcal{S}$ ). It is naturally of interest to explore how the transition from adiabatic to nonadiabatic occurs. To that effect we show in Fig. 9 the period ratios as a function of the logarithm of the nonadiabaticity parameter  $\epsilon$  (We use the same definition as Zalewski 1992; *viz.* in the dynamical equation  $\epsilon$  multiplies the entropy contribution to the pressure variation in the mechanical equation,  $\epsilon=0$  thus being the adiabatic case and  $\epsilon=1$  being the full nonadiabatic one).

Note that it is indeed for the strange modes that the period ratio changes most rapidly in Fig. 9. The rea-

**Table 1.** Comparison of exact and adiabatic periods  
From left to right: mode, period, growth-rate, moment of inertia, adiabatic period; the strange mode is indicated with S.

mode	$P_n$ [d]	$\eta_n$	$I_n$	$P_n^{ad}$ [d]
F	9.089	0.018	2.10e+30	9.145
O1	6.278	0.054	4.71e+29	6.324
O2	4.525	-0.121	4.18e+29	4.507
O3	3.554	-0.291	4.39e+29	3.517
O4	2.937	-0.371	3.29e+29	2.885
O5	2.494	-0.313	2.06e+29	2.437
O6	2.164	-0.207	9.42e+28	2.109
O7	1.907	-0.100	2.21e+28	1.853
O8	<sup>s</sup> 1.729	0.209	1.60e+27	1.650
O9	1.649	-0.261	1.88e+27	1.489
O10	1.534	-0.319	5.38e+27	1.362
O11	1.400	-0.232	1.55e+28	<sup>s</sup> 1.281
O12	1.285	-0.215	1.76e+28	1.219
O13	1.193	-0.177	8.70e+27	1.139
O14	1.135	-0.181	4.88e+27	1.063

son for this extreme sensitivity is also clear. The resonance condition is very sensitive to the outer region. But there the Cepheid envelope is highly nonadiabatic (e.g. Cox 1980) even though, overall, the Cepheid pulsation is weakly nonadiabatic, as already pointed out. It is therefore expected that even a small nonadiabaticity can have the dramatic effect of gradually shifting the strange mode from O11 down to O8 as Fig. 9 indicates.

## 5. Cepheid Sequence

We now turn to a Cepheid model sequence with  $M=5M_{\odot}$ ,  $L=3000L_{\odot}$ ,  $X=0.7$ ,  $Z=0.02$ , in which the variable parameter is the fundamental period  $P_0$ , or equivalently the  $T_{eff}$  ranging here from 8600 K to 4600 K. We have chosen this somewhat overluminous sequence (on the Chiosi  $M-L$  relation) simply because the strange mode appear as a vibrational overtone with lower modal number.

### 5.1. Modal spectrum

We start again by examining the adiabatic models, and show in Fig. 10 the behavior of the adiabatic period ratios  $P_{n0} = P_n/P_0$  for the model sequence. The adiabatic modes are seen to display avoided level crossings. Here we can prove that the levels cannot cross. Indeed, because of the Sturm-Liouville nature of the adiabatic eigenvalue problem (e.g. Ledoux & Walraven 1958) the modes have distinct frequencies – no degeneracy and no crossings.

Guided by the toy problem (Figure 3) we understand that the level crossings are a consequence of the relative shift in the location of the potential barrier, and thus

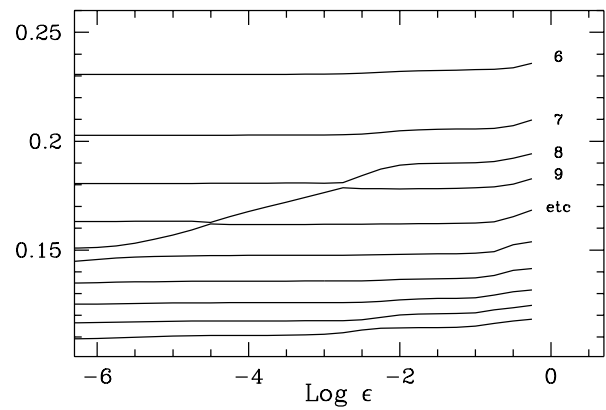


**Fig. 9.** Period ratios  $P_{n0}$  in the transition from adiabatic to nonadiabatic model as a function of  $\text{Log}(\epsilon)$ , where  $\epsilon$  is the nonadiabaticity parameter

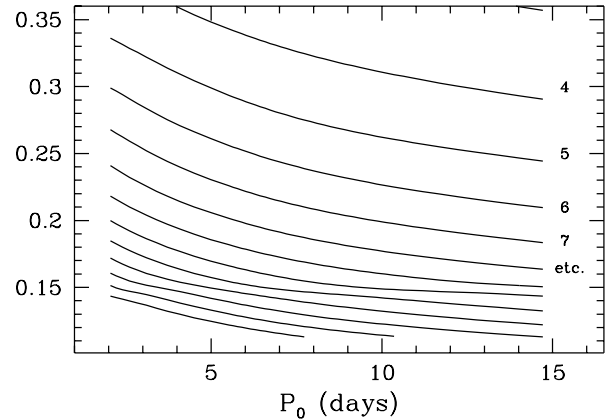


**Fig. 10.** Cepheid model sequence; Period Ratios  $P_{n0}$  of the adiabatic spectrum based on the first fifteen overtone modes of the spectrum ( $k=1, 15$ ); only ratios with  $k > 3$  are shown.

in the resonance condition. Indeed with increasing period (or decreasing  $T_{eff}$ ) the HPIR moves inward, causing the strange mode to move to lower modal number. As we go from high to low  $T_{eff}$  (low to high  $P_0$ ) the HPIR moves inward, and concomitantly the outer potential well increases in width relative to the inner one. In the toy problem this corresponds to decreasing  $z_o$ . We therefore anticipate a behavior comparable to that of the toy problem displayed in Fig. 3.

Turning now to the full *nonadiabatic* models we plot in Fig. 11, on top, the period ratios which also show avoided crossings. However, they are shifted with respect to the nonadiabatic picture and are more dramatic. The mode labelled 15 on the left successively trades places with modes 14, 13, 12, etc and ends up as mode 7 on the right side of the figure.

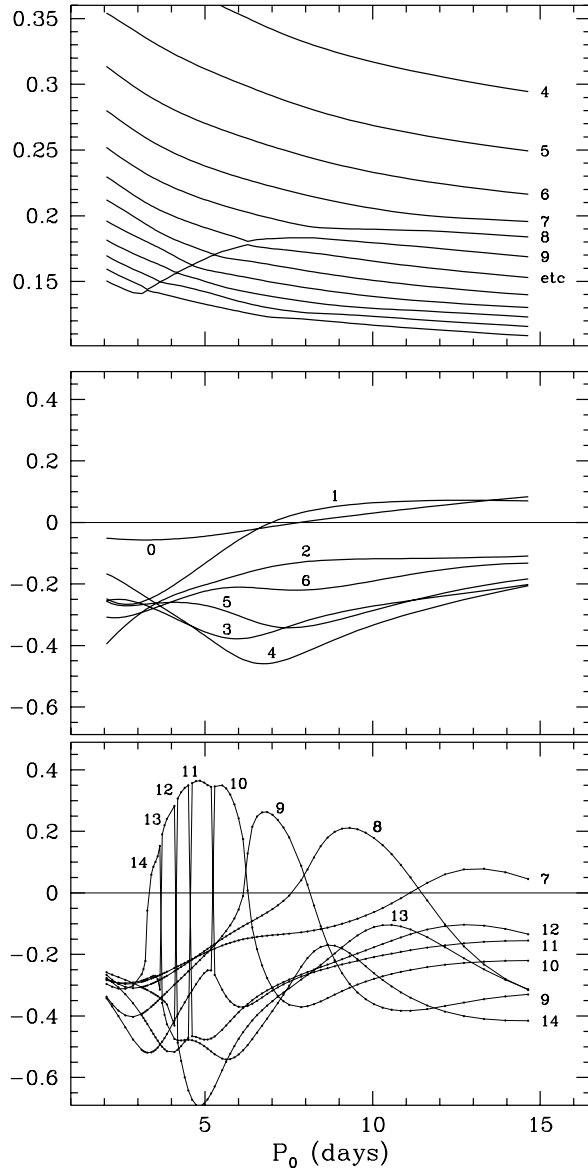


**Fig. 11.** Nonadiabatic Cepheid model sequence, *top*: Period ratios,  $P_{n0,k}=1,14$ ; *middle*: relative growth-rates,  $k=0,6$ ; *bottom*: relative growth-rates,  $k=7, 12$ ; individual models are indicated by points in the bottom graph.

The middle and bottom graphs in Fig. 11 display the relative growth-rates  $\eta_n = 2\kappa_n P_n$ , for modes  $k=0$  through 6, and  $k=7$  through 14, respectively. Thus the first overtone in this sequence is unstable for  $T_{\text{eff}} < 6000$  K ( $P_1 = 4.7$  d) and the fundamental for  $T_{\text{eff}} < 5800$  K ( $P_0 = 7.7$  d).

In the bottom graph that shows the higher overtones we witness some interesting behavior. The lines connect the points ordered by decreasing  $P_{n0}$  which is different from the way the eye connects them. There is an unstable modal feature throughout the whole period range, but it is not always the same mode. Furthermore whenever a level crossing occurs in the top graph, there is a corresponding

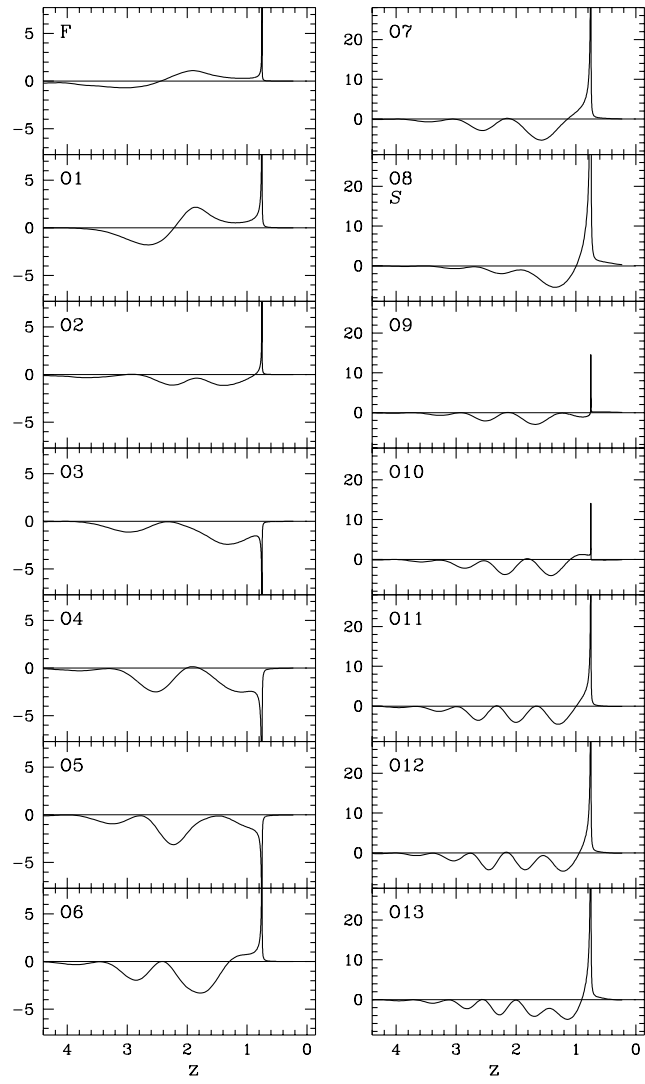


**Fig. 12.** Work integrands vs. acoustic depth for Cepheid Model; the strange mode is labelled by  $S$ .

switch-over in the growth-rates of the two corresponding modes. The switch-over is relatively slow for modes 7 to 8 and 8 to 9, more rapid for modes 9 to 10 and 10 to 11 and very rapid for the higher modes. (The reason is simply that the position of the HPIR moves more rapidly with  $P_0$  for low  $P_0$ .) In both the period ratios and in the growth-rates it is as if some egregious modal property hops from mode 14 to mode 7.

A more careful inspection of Fig. 11 uncovers among the higher modes the appearance of a second strange mode in the period ratios. Some secondary structure is even more clearly visible in the growth-rates. There are local maxima for modes 13 and 14 at  $10^{4.5}$  and  $8^{4.5}$  days, respectively, which are due the appearance of higher order strange modes – by which it is meant that a second node crosses the HPIR.

In a recent paper Glasner & Buchler (1993) already noted that for RR Lyrae and Cepheid models the stability of the vibrational modes does not increase monotonically with mode number. Instead, there is a strong excursion back toward instability around the eighth or ninth overtone. At the time they had no physical explanation for the nonmonotone behavior, but the present results show that this is related to the recurrent appearance with increasing modal number of strange modes.

### 5.2. Work-integrands

Fig. 11 shows that the strange mode has a very different growth-rate from its neighbors and it is interesting to inquire why. In Fig. 12 we therefore examine the work integrands, *i.e.* the work  $\langle pdv \rangle$  done per cycle, or the integrand of the expression for the relative growth-rate

$$\begin{aligned} \eta_n &= 2 \frac{\kappa_n}{\omega_n} = \frac{2\pi}{\omega_n^2 I_n} \operatorname{Im} \int \delta p_n \delta v_n^* 4\pi r^2 \rho c_s dz \\ &= \frac{2\pi}{\omega_n^2 I_n} \int \Delta p \Delta v \sin(\phi_p - \phi_v) 4\pi r^2 \rho c_s dz \end{aligned} \quad (15)$$

where the  $\phi_p$  is the phase of  $\delta p_n$  and  $\Delta p_n$  its modulus, and similarly for the specific volume eigenvector  $\delta v$ . The quantity  $\eta_n$  represents the energy growth of a mode over one period – its inverse is equal to the quality factor  $Q_n$  commonly associated with resonant electronic devices. The quantity  $I_n$  is the moment of inertia of the mode:

$$I_n = \int |\delta r_n|^2 dm \quad (16)$$

(*e.g.* Glasner & Buchler 1993). A positive work-integrand means that locally internal energy is converted into kinetic (pulsational) energy.

In Fig. 12 we exhibit the work-integrands for the lowest 14 modes as a function of  $z$  (The areas under the curves are the relative growth-rates). It is apparent in Fig. 12 that the egregious growth-rate of the strange mode is the result of two effects. First, the inner pulsation amplitude that we have shown to be characteristic of the strange mode causes both  $\Delta p$  and  $\Delta \rho$  and hence the integral (eq. 15) to be much smaller for the strange mode. Thus the surface region plays a relatively larger role in the growth-rate. Second, the smallness of the integral is compensated for by the considerable amplification that comes about from the small moment of inertia  $I_n$  in the denominator of Eq. 15. The resulting strange growth-rate is therefore largely the result of the contribution from the outer region. In this example, the outer region happens to be driving, this is the source of the positive growth rate of the strange mode.

Since for the strange modes almost all of the driving comes from the HPIR the stability of these modes is therefore more sensitive to the physical and numerical resolution of the outer layers. However, as we have seen, their existence and nature are not sensitive at all.

More light can be shed on the behavior of the growth-rates by examining a non-adiabatic extension of our toy model, which we consider next.

### 6. Nonadiabatic Toy Potential Barrier Problem

The nonadiabatic problem is of course much more complicated, but it is possible to extend the potential barrier problem of §2 to mimic nonadiabatic pulsations by generalizing Eq. 9:

$$-\tilde{y}'' + \mathcal{V} \tilde{k} \delta(z - z_o) \tilde{y} + iU \tilde{y} = \tilde{\omega}^2 \tilde{y} \quad (17)$$

where  $\tilde{k}$  is the (complex) wave-vector  $\tilde{k} = \sqrt{(\tilde{\omega}^2 - iU)}$ , and  $\tilde{\omega}$  is the complex frequency. The potential  $U$  mimics an overall dissipation. In the adiabatic case,  $\mathcal{V}$  was a real constant of value  $V_o$ . Here we extend the potential to include an imaginary component  $\mathcal{V} = V_o + i\Delta V_o$ . The choice of  $\Delta V_o$  represents a crude solution of the nonadiabatic pulsation equations:

$$\tilde{\omega}^2 \delta r = G_1 \delta r + G_2 T \delta s, \quad (18a)$$

$$i\tilde{\omega} T \delta s = K_1 \delta r + K_2 T \delta s, \quad (18b)$$

in which we assume that  $(G_2(i\tilde{\omega} - K_2)^{-1}K_1) \delta r$  can be replaced with a complex term  $\mathcal{B} \delta r$ , proportional to  $\delta r$  and thus to  $y$ . It has been recognized that the shape of the entropy fluctuations is independent of the mode (Pesnell & Buchler 1986) and is well represented by a sharp peak in the ionization region. As a result we superimpose the complex  $\Delta V_o$  onto the adiabatic delta function potential.

The inner boundary condition is still  $\tilde{y}(0) = 0$ , but the outer one can now be more general (*e.g.* Morse & Feshbach, 1953, Eq. 11.1.21 ff), *viz.*  $\delta p = R\dot{u} + Xu$  which translates here into  $\tilde{y}'(1) = \mathcal{Z}y(1)$ , where  $\mathcal{Z}$  is a complex surface impedance.  $\mathcal{Z} = 0$  corresponds to a free surface as in the adiabatic case (perfect reflection).  $\operatorname{Im} \mathcal{Z}$  is the inertia presented to the stellar surface by an overlying atmosphere, and  $\operatorname{Re} \mathcal{Z}$  corresponds to acoustic radiation losses.

For highly nonadiabatic stars the adiabatic potential barrier that is contained in  $G_1$  becomes less important relative to the second term, and it is the  $\delta$  function from the peaking of  $\delta s$  that dominates the problem. We note in passing that Zalewski (1992) decided to include an inhomogeneous term  $A\delta(z - z_o)$  instead of a potential, and took  $\mathcal{Z}$  to be a real constant  $v_0$  (whose value he did not specify in the paper). His simple model does not work for Cepheids although it matches some, but not all the properties of the spectrum of the highly nonadiabatic PAGB models.

With the appropriate matching conditions  $y(z_o^+) = y(z_o^-)$  and  $\tilde{y}'(z_o^+) = \tilde{y}'(z_o^-) + \tilde{k} \mathcal{V} \tilde{y}(z_o)$ , one obtains the eigenvalue equation for the complex wave-vector  $\tilde{k}$

$$\begin{aligned} \cos \tilde{k} - \mathcal{Z} \sin \tilde{k} \\ = -V_o \sin \tilde{k} z_o (\cos \tilde{k}(1 - z_o) - \mathcal{Z} \sin \tilde{k}(1 - z_o)) \end{aligned} \quad (19)$$

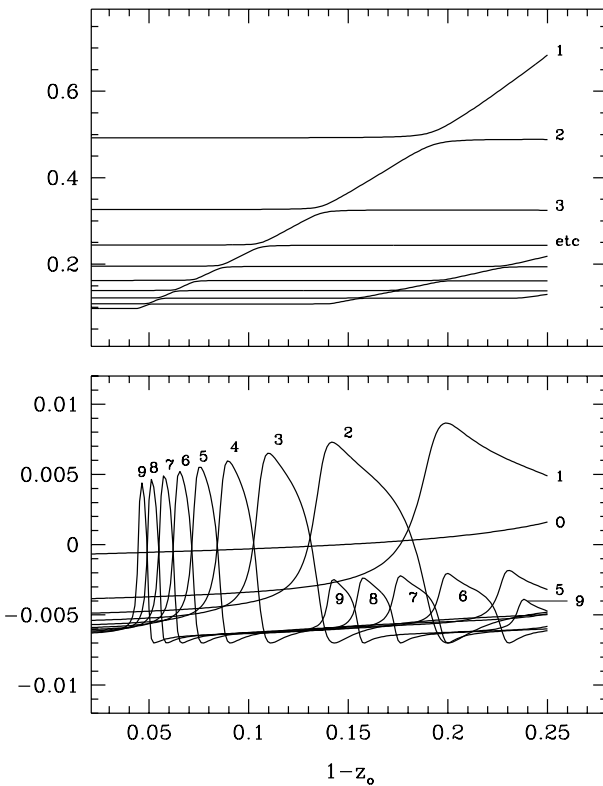


**Fig. 13.** Period ratios (top) and relative growth-rates (bottom) as a function of outer well width  $1-z_o$  for the lowest 9 modes of the complex barrier problem with  $\mathcal{V} = 10 - 2i$ ,  $U = 0.02$ .

The solution is given by

$$\begin{aligned} \tilde{y}(z) &= a \sin \tilde{k}z & z \leq z_o \\ &= \cos \tilde{k}(1-z) - \mathcal{Z} \sin \tilde{k}(1-z) & z_o \leq z \end{aligned} \quad (20)$$

where the inner amplitude  $a(\tilde{k}) = y'(0)/\tilde{k}y(1)$  is now

$$a(\tilde{k}) = (\cos \tilde{k}(1-z_o) - \mathcal{Z} \sin \tilde{k}(1-z_o))/\sin \tilde{k}z_o \quad (21)$$

Again, we examine a sequence of toy models, but this time for a relatively narrow range of barrier locations,  $z_o$ . We have chosen the parameters  $\mathcal{V} = 10 - 2i$  and  $U = 0.02$ . We set  $\mathcal{Z} = 0$  consistent with  $p_* \approx 0$ , as in the hydrocode. The period ratios for this sequence are shown in Fig. 13 (top) and it is easy to follow the strange property from overtone 9 at the bottom left corner to overtone 1 at the top right. In Fig. 13 (bottom) we show the corresponding growth-rates of the lowest modes, as obtained with Eq. 19.

Considering the crudeness of the toy model's  $\delta$  function potential, the properties of the growth-rates mimic those of the Cepheid sequence remarkably well. Here, as in Fig. 11, we see the increasingly rapid switchover of the unstable excursions and even, at bottom right, the weaker excursions of the second and third order strange modes. In this toy model, the effect of second and third order strange

modes are also visible in the period ratios (Fig. 13 top) as it was in the Cepheid sequence (Fig. 11).

The behavior of our eigenvalues can actually be understood analytically via perturbation theory when the nonadiabaticity is small. The correction  $\Delta\omega^2$  (where  $\tilde{\omega}^2 = \omega^2 + \Delta\omega^2$  to first order) to the eigenvalue due to the complex potential  $U$  and the small imaginary contribution to  $\mathcal{V}$  is given in terms of unperturbed (adiabatic) quantities

$$\begin{aligned} \Delta\omega^2 &= iU + i\Delta V_o k y^2(z_o)/\mathcal{I} \\ &= iU + i\Delta V_o a(k)^2 \sin^2 k z_o/\mathcal{I} \end{aligned} \quad (22)$$

where  $\mathcal{I} = \int |y|^2 dz$ . The correction is seen to be at a *maximum* for the strange mode for which  $\mathcal{I}$  is at a *minimum*. In contrast, it is at a *minimum* for the neighboring matched mode for which  $y(z_o) \approx 0$ . This explains the rapid variation of the growth-rates in the vicinity of the strange modes. Fig. 13 confirms both of these predictions. The potential  $U$  by construction provides an overall shift of  $\text{Im } \omega$  to negative values.

## 7. The Cepheid Horn

The reduction of the adiabatic pulsation problem to a Schrödinger like equation is very well known in the study of wind instruments (Morse & Ingard 1968, Benade 1977). But it is common to focus on pressure perturbations, though it is straightforward to show the equivalence of the following two descriptions of linear sound waves in a horn, the first for the velocity perturbation  $u$  (or equivalently for  $\delta r$ ), and the second, well known Bernoulli-Webster equation, for the pressure  $\delta p$

$$\frac{1}{\rho} \frac{\partial}{\partial x} \left( \frac{\rho c_s^2}{S} \frac{\partial}{\partial x} (S u) \right) = \omega^2 u, \quad (23)$$

$$\frac{c_s^2 \rho}{S} \frac{\partial}{\partial x} \left( \frac{S}{\rho} \frac{\partial}{\partial x} \delta p \right) = \omega^2 \delta p, \quad (24)$$

In the case of an acoustic horn it is not usually necessary to consider gradients in the sound speed  $c_s$  and density  $\rho$ , and it is the *shape of the spatially varying cross-sectional area  $S(z)$*  that determines the potential  $V(z)$ .

Eq. (23) can be transformed into a Schrödinger equation of the form (Eq. 7) in the same way as Eq. (1), in which the potential is

$$V_u(z) = (S/\rho)^{\frac{1}{2}} \frac{d^2}{dz^2} (S/\rho)^{-\frac{1}{2}}. \quad (25)$$

*Mutatis mutandis*, the potential for Eq. (12) is shown to be

$$V_p(z) = (S/\rho)^{-\frac{1}{2}} \frac{d^2}{dz^2} (S/\rho)^{\frac{1}{2}}. \quad (26)$$

The potential  $V_p(z)$  is the so called *horn function* (Morse & Ingard 1968, Benade 1977). (We note in passing that a standard reference to the Webster-Bernoulli equation, *viz.*

Eq. 1 in Eisner (1967) incorrectly uses Eq. (24) instead of Eq. (23) as the equation for the displacement.)

In the case of the horn it is the curvature associated with the flaring that can give rise to potential barriers. Reflection at these barriers (often phrased in terms of acoustic impedance mismatch) produces internally trapped modes, which are the discrete tones of the horn or wind instrument in question. In contrast, loudspeaker horns are flared exponentially so as to avoid potential barriers.

Can we design a wind instrument with a flare function  $\mathcal{R}(z) = \sqrt{S(z)}$  chosen so as to have the same acoustic spectrum as our variable star? In the Cepheid, as we have seen, the potential is produced by the variation of  $\rho$ ,  $c_s$ , the spherical geometry, and by gravity. Can we work backwards from the potential of Eq. (8) to find the shape  $\mathcal{R}(z)$  of horn that would reproduce a Cepheid's tones?

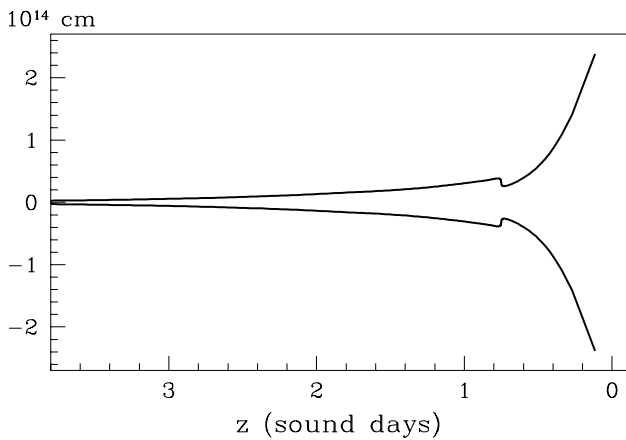


**Fig. 14.** Cross-section of the horn corresponding to Cepheid pulsations, shown over the outer portion of the pulsating envelope (The entire model envelope extends to  $z = 8$ ); the kink at  $z = 0.75$  corresponds to the potential barrier.

A closer inspection of the stellar problem shows immediately a big difference with a horn, aside from the strong spatial gradients of density and sound speed: The potential  $V$  in Eq. (8) contains a gravitational term that cannot be absorbed away into the term that has the form of a horn function. The presence of the gravitational potential term thus makes the inversion from the potential to the flare function impossible unless a Cowling approximation is made.

With the Cowling approximation we can construct an approximate equivalent acoustic horn – with the horn part being of primary importance everywhere except in the innermost regions of the star. In Fig. 14 we show a slice through the horn that would produce the same horn function as the Cepheid model (with  $T_{\text{eff}} = 5520$  K). The modes produced by this horn of course have somewhat different periods from the original Cepheid because of the Cowling

approximation. It is indeed well known that this approximation is not very accurate for low radial modes, and the reason has already been mentioned: The nodal structure is determined by the whole envelope, as the transformation to  $z$  has shown particularly clearly. Nevertheless, it is amusing to see that in the region where the horn function dominates the potential, a constriction in the bell of the horn arises because of the HPIR.

Because the strange modes are trapped surface modes they should feel very little the gravitational potential. They can therefore well be described with the horn potential only. Interestingly the radial displacement eigenvectors have an appreciable amplitude only in the outer, open part of the flare.

## 8. Nonlinear Pulsations

The strange modes are seen to be unstable to the left of the blue edge of the fundamental mode and the first overtone – in fact the strange mode can be the only unstable vibrational mode there (Fig. 11). It is of course interesting to investigate what the pulsations of this star look like and why no observational evidence has been reported for variability in this region of the HR diagram.

We have seen in Fig. 8 that the region outside the HPIR dominates the radial eigenvectors and thus the pulsation. *A priori* we have no idea of what the amplitude of pulsation might be. We have therefore computed the nonlinear (limit cycle) pulsations of several models from our sequence, that are located to the left of the Cepheid instability strip (and are therefore not Cepheids *stricto sensu*).

For all these models the limit cycle pulsations have a very small amplitude, typically 0.1 – 1 km/s photospheric velocity and magnitude variations of milli-mags. If such 'strange Cepheids' indeed exist they are very hard to detect. Aikawa & Sreenivasan (1995) have found similarly small amplitudes for yellow supergiant and intermediate mass stellar models pulsating in a strange mode.

The effects of the strange mode might also be felt directly in the regime of normal Cepheids. Two simple scenarios are possible here in theory: (a) the strange mode is linearly unstable together with the fundamental (or with the first overtone); if the nonlinear coupling coefficients happens to have suitable values, then beat pulsations can occur (The conditions that must be satisfied are described in great detail in Buchler & Kovács 1986); (b) the strange mode is resonant through a higher order resonance, say 4:1 or 5:1, cf. Fig. 11, top). If the strange mode is further linearly unstable or just marginally stable and the nonlinear coupling coefficients are right, then periodic, frequency locked pulsations can occur (irregular amplitude modulations are also possible in principle, but less likely). Finally, the strange modes could have an indirect effect in that they could destabilize the fundamental (or first

overtone) limit cycles in a regime where the first overtone (or fundamental) limit cycles are also unstable. The result would then be a usual beat Cepheid, i.e. constant amplitude pulsations in both the fundamental and first overtone (Buchler 1997).

For the strange modes to be able to have any of the described effects depends on the strength of the nonlinear coupling coefficients. Whether the small overlap between the normal and the strange modes allows a strong enough coupling is unknown at present. Hydrodynamic computations are in progress to explore these phenomena.

## 9. Conclusions

We have shown that the problem of adiabatic radial pulsations can be very instructively recast in terms of a Schrödinger equation – this without any approximations. The sharp variations in sound speed through the hydrogen partial ionization region create a very high and very narrow potential barrier, separating the pulsating envelope into two regions. The appearance of strange modes is a consequence of the possibility of mode-trapping in the surface regions.

While this Schrödinger equation formulation is strictly correct only in the adiabatic limit, the same phenomenon of trapping persists when nonadiabatic effects and acoustic radiative losses are taken into account.

It is clear from our study that the strange modes are thus of acoustic origin, rather than arising as a coalescence of two thermal or secular modes.

The phenomenon of trapping has been illustrated with a simple analytical toy problem that exhibits all the important features associated with the strange modes, such as avoided level crossings. This model can also be extended to explain the properties of the nonadiabatic spectrum. The resemblance with the behavior of the periods and growth-rates of a Cepheid model sequence is striking.

There is of course no reason why strange modes should not occur in the nonradial spectrum of low  $\ell$   $p$  modes, because these modes feel essentially the same potential as the radial modes (although a Schrödinger formulation is no longer possible without approximation because of the higher order of the nonradial equation). The level crossings are therefore distinct from those that occur when  $p$  and  $g$  modes interact (Unno et al. 1989).

Finally, we have examined the nonlinear pulsations associated with the strange modes and have concluded that they have very small amplitudes, especially in luminosity.

We wish to thank Art Cox for his comments on this paper. This work has been supported in part by NSF (grants AST92-18068, INT94-15868 and AST95-28338).

## References

Aikawa, T. 1985, *Ap & Space Sci.* 116, 401  
 Aikawa, T. & Sreenivasan, S. R. 1996, *PASP* 107, 238  
 Alexander, D. R., Ferguson, J. W. 1994, *ApJ* 437, 879  
 Benade, A. H. 1977, in *Musical Acoustics*, Ed. E.L. Kent (Dowden, Hutchinson & Ross: Stroudsburg, PA), p. 110  
 Buchler, J.R. 1997, in "Astrophysical Fallouts From Microlensing Projects", Eds. R. Ferlet J.P. Maillart & B. Raban, Editions Frontières, Gif-s-Yvette  
 Buchler, J. R. & Kovács, G. 1986, *ApJ*, 303, 749  
 Cox J. P. 1980, *Stellar Pulsations*, Princeton Univ. Press  
 Cox, J. P. & Giuli R. T. 1969, *Principles of Stellar Structure* (New York: Gordon and Breach)  
 Cox, J. P. & Guzik, J. A. 1996, in "Luminous Blue Variables: Massive Stars in Transition," Eds. A. Nota & H. Lamers  
 Cox, J. P., King, D. S., Cox, A. N., Wheeler, J. C., Hansen, C. J. & Hodson, S.W. 1980, *Space Sci. Rev.* 27, 529  
 Deubner, F.-L. & Gough, D. 1984, *Ann. Rev. Astr. Astrophys.* 22, 593  
 Eisner, E. 1967, *J. Acoust. Soc. Am.* 41, 1126–1146  
 Fraley, G. S. 1968, *Ap&SS*, 2, 96  
 Gautschy, A. & Glatzel, W. 1990, *MNRAS* 245, 597  
 Glasner, A. & Buchler, J. R. 1993, *A&A*, 227, 69  
 Glatzel, W. 1994, *MNRAS* 271, 66  
 Iglesias, C.A. & Rogers, F. J., 1996, *ApJ*, 464, 943  
 Ledoux, P. & Walraven, T. 1958, in *Handbuch der Physik*, ed. S. Flügge (Berlin : Springer), 51, 353  
 Morse, P.M. & Ingard, K.U., 1968, *Theoretical Acoustics*, McGraw-Hill : New York  
 Morse P.M. & Feshbach, H. 1953, *Methods of Theoretical Physics*, (McGraw Hill, NY)  
 Papaloizou, J.C.B., Alberts, F., Pringle, J.E., Savonije, G.J. 1997, *MNRAS* 284, 821–829  
 Pesnell, W.D. & Buchler, J.R. 1986, *ApJ*. 303, 740  
 Saio, H., Wheeler, C.J. & Cox, J.P. 1984, *ApJ* 281, 318  
 Unno, W., Osaki, Y., Ando, H., Saio, H., & Shibahashi, H. 1989, *Nonradial Oscillations of Stars*, Univ. of Tokyo Press  
 Zalewski, J. 1992, *PASJ* 44, 27